Available online at www.sciencedirect.com

ScienceDirect

Proceedings of the Combustion Institute 35 (2015) 3201–3208

Proceedings of the Combustion Institute

www.elsevier.com/locate/proci

Wall-temperature effects on flame response to acoustic oscillations

D. Mejia [a], L. Selle [a,b,*], R. Bazile [a], T. Poinsot [a,b]

[a] Université de Toulouse, INPT, UPS, IMFT (Institut de Mécanique des Fluides de Toulouse), Allée Camille Soula, F-31400 Toulouse, France

[b] CNRS, IMFT, F-31400 Toulouse, France

Available online 26 July 2014

Abstract

This paper presents an experimental investigation of combustion instabilities for a laminar premixed flame stabilized on a slot burner. For certain operating conditions, the system exhibits an unstable mode locked on the Helmholtz mode of the burner. It is shown that the instability can be controlled and even suppressed by changing solely the temperature of the burner rim. A theoretical model accounting for this parameter in the flame transfer function is devised and the physical mechanisms for the temperature dependance of the flame response are investigated.

Keywords: Combustion instabilities; Flame transfer function; Wall temperature

1. Introduction

The occurrence of combustion instabilities (CI) is a major problem for the design and operation of many power-generation systems such as gas turbines, aeronautical engines and rocket engines [1]. The constructive coupling between acoustic waves and unsteady heat release rate constitutive of CI is responsible for loss of performance, restriction in operating conditions and sometimes catastrophic failures. The challenge for understanding and predicting CI lies in the multiplicity of physical phenomena involved in the unstable loop [2]: acoustics, vortex dynamics, mixing, chemistry, two-phase flows, etc. One of the canonical configurations for the study of CI is the laminar premixed flame, which has been extensively studied [3–5]. Recent theoretical developments [6,7] propose analytical solutions for the flame response to acoustic perturbation, which is a central element for the prediction of CI. For linear-stability analysis, the flame response is assumed to depend only on the frequency of the incident perturbations, nevertheless its response may depend on many other parameters. The present study focuses on the impact of heat transfer on the flame response, based on the experimental observation that most systems behave differently at cold start and in the permanent regime. We therefore investigate the response of a laminar premixed flame where the temperature of the

* Corresponding author at: Université de Toulouse, INPT, UPS, IMFT (Institut de Mécanique des Fluides de Toulouse), Allée Camille Soula, F-31400 Toulouse, France.

E-mail address: laurent.selle@imft.fr (L. Selle).

http://dx.doi.org/10.1016/j.proci.2014.07.015
1540-7489/

burner at the flame anchoring point can be controlled and monitored.

The manuscript is organized as follows: in Section 2 the experimental setup and diagnostics are presented, while Section 3 presents a self-sustained CI, dependent on the burner-rim temperature. Section 4 is devoted to the derivation of a low-order model for the prediction of the stability map and the input parameters for this model are measured in Section 5. Finally, in Section 6 the impact of the flame-root dynamics on the overall flame response is scrutinized.

2. Experimental setup and diagnostics

The experiment is a slot burner [8] with a laminar premixed methane/air flame stabilized at the burner outlet (*cf.* Fig. 1). The four main components are: a mixing chamber, a plenum, a convergent nozzle and a rectangular-cross-section slot (width $w_s = 10$ mm and length $l_s = 100$ mm) with a height $h_s = 70$ mm. The flow rates of air and methane are controlled and measured via individual mass flow meters: Bronkhorst F-201 AV-AAD-33-V. The reactants are injected at the bottom of the mixing chamber in a cross-flow configuration to maximize mixing. The premixed flow is then laminarized in the plenum by an array of small glass balls and three honeycomb panels. Finally, it passes through the converging nozzle and the slot. The level of premixing is excellent as the flame shape is regular and steady. In order to control the temperature of the burner rim, the long sides of the slot are water-cooled by two pairs of cylindrical passages (*cf.* Fig. 2) with a

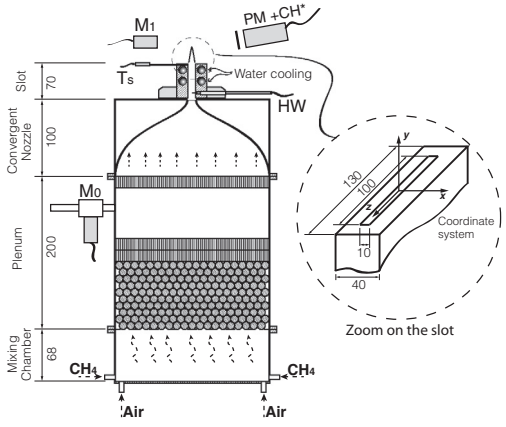

Fig. 1. Sketch of the burner: transverse cut and experimental diagnostics. The four main components are: the mixing chamber, the plenum, the nozzle and the slot. M_0 and M_1 are 1/2″ microphones. PM + CH^* is a photomultiplier equipped with CH^* filter. HW corresponds to a hotwire. T_W is K-type thermocouple.

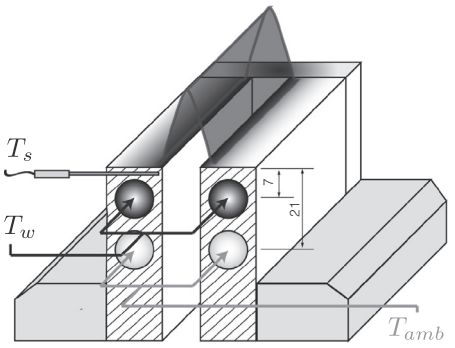

Fig. 2. Perspective view of the slot with a cut through the material at $z = 0$. The upper and lower cooling channels allow a water flow at T_w and T_{amb}, respectively.

5 mm cross-section, centered 7 mm and 21 mm below the burner rim, *i.e.* at $x = \pm 12.5$ mm, $y = -7$ mm and $y = -21$ mm in the reference coordinates of Fig. 1. The water temperature, T_w, in the upper channels ($y = -7$ mm) can be set between 1 and 99 °C, with a mass flow rate up to 1 kg/min. In the lower channels ($y = -21$ mm) water at ambient temperature flows at 5 kg/min. A K-type thermocouple is placed 1 mm below the burner outlet ($x = -6$ mm, $y = -1$ mm and $z = 0$ mm). It gives the temperature, T_s, of the material as close as possible to the flame base. The purpose of this dual-channel cooling system is to be able to control T_s, while maintaining the lower part of the slot and the burner under ambient conditions.

A hot wire probe, labeled HW in Fig. 1, is used to measure the unsteady axial velocity $v_1(t)$, located 55 mm upstream of the slot outlet ($x = 0$ mm, $y = -55$ mm and $z = 0$ mm). A photomultiplier, labeled PM in Fig. 1, measures the unsteady intensity, $I(t)$, of spontaneous emission of CH^* radicals. The PM is equipped with a narrow-band filter centered on a wavelength $\lambda = 430$ mm and is placed 400 mm away from the flame, aligned with the z axis ($x = 0$ mm, $y = 10$ mm and $z = 400$ mm), facing the longitudinal axis of the flame, which is fully included in its field of view. It has been shown that for lean premixed flames, $I(t)$ is proportional to the heat release rate [9]. Two microphones, M_0 and M_1, are used to record the acoustic pressure fluctuation, $p'_0(t)$ and $p'_1(t)$, respectively. M_0 is placed in a waveguide connected to a pressure plughole in the middle of the plenum ($x = -100$ mm, $y = -270$ mm and $z = 0$ mm), while M_1 is located 300 mm away from the burner ($x = 0$ mm, $y = 10$ mm and $z = 300$ mm). For forced experiments the bottom of the plenum can be replaced by a 130 mm loudspeaker driver by a signal generator. A high-speed camera (pco.dimax) is used to track the flame root when submitted to an acoustic modulation. The camera is equipped with a

Micro-Nikkor $f/2.8$ 105 mm Nikon lens, located at $x = 0$ mm, $y = 10$ mm and $z = 350$ mm. Images zoomed on the flame base of 624-by-928 pixel with a resolution of 70 px/mm were acquired at a sampling frequency of $f_{cam} = 3000$ fps and an exposure time of 0.30 ms, during 2 s. For each pulsating frequency, 6000 images are acquired. A LabVIEW program is used as a signal generator, to drive the loudspeaker at the bottom of the burner and to send a synchronized TTL signal to trigger the camera. Thanks to this synchronization, the images can be phase-averaged with respect to the acoustic modulation.

3. Description of the unstable behavior

Configurations similar to Fig. 1 typically exhibit instabilities locked on the Helmholtz mode of the cavity [10–12]. For a given flame, which has its own response to acoustic perturbations, stability depends on the Helmholtz frequency and the level of dissipation in the system. Because of its direct impact on both effects, the main parameter controlling the occurrence of instabilities is the height, h_s, of the slot [13].

In this study, however, an other parameter has been identified: the temperature, T_s, of the burner rim. Indeed, for a slot height $h_s = 70$ mm, the flame is unstable when the slot is cold and stable once hot. This behavior is illustrated in Fig. 3, which presents the joint evolution of pressure fluctuation in the plenum and slot temperature versus time. The operating point for this test is an equivalence ratio $\Phi = 0.95$ and a bulk velocity in the slot $\bar{u} = 1.6$ m/s. Temperature and pressure correspond to ambient conditions $T_{amb} = 20$ °C and $P_{amb} = 0.993$ bar, respectively. As shown in Fig. 3, at $t = 0$, the whole experiment is at ambient temperature and the cooling system is off. Combustion is initiated at $t = 20$ s and an instability develops immediately at a frequency $f_r = 58$ Hz, corresponding to the Helmholtz mode of the burner (*cf.* Section 4). The pressure fluctuation inside the plenum reaches 113 dB and decreases gradually as the slot temperature, T_s, increases. Around $t = 300$ s, the instability reduces drastically and the flame is fully stable past $t = 400$ s. Meanwhile, T_s is over 100 °C and still increasing. At $t = 480$ s, the cooling system is started with water at $T_w = 3$ °C flowing through the slot, resulting in a sharp drop of T_s. The instability rises back up and the whole system reaches a steady state around $t = 800$ s, with $\|p_0'\| = 110$ dB and $T_s = 50$ °C. This behavior is fully repeatable and the instability can be controlled only using the cooling system, demonstrating that the burner-rim temperature is one of the parameters controlling the instability. To study the transition between stable and unstable modes, a quasi-steady-state analysis was performed. By varying the cooling-water temperature and waiting for a steady state, one can determine the amplitude of the instability versus slot temperature. The relative velocity fluctuation, $\varepsilon = v_1^{rms}/\bar{v}$, and heat release rate fluctuation, $\sigma = I^{rms}/\bar{I}$, are presented in Fig. 4 versus T_s. With maximum cooling, corresponding to $T_s = 48$ °C, ε and σ reach as much as 10%. For $T_s = 60$ °C the fluctuation levels are down to 5% and lower than 1% past $T_s = 70$ °C. The instability is shut down by increasing the wall temperature by less than 20 °C, showing how sensitive flames are to heat transfer.

4. Low-order model

Because the instability described in Section 3 is locked on the Helmholtz mode of the burner, one can derive an analytical model as described in [10]. For harmonic perturbations, $v_1' = \|v_1'\|e^{-i\omega t}$, Eq. (6) in [10] reduces to an equation for the pulsation ω:

$$\left[1 + Cne^{i\omega\tau}\right]\omega^2 + 2i\delta\omega - \omega_0^2 = 0 \qquad (1)$$

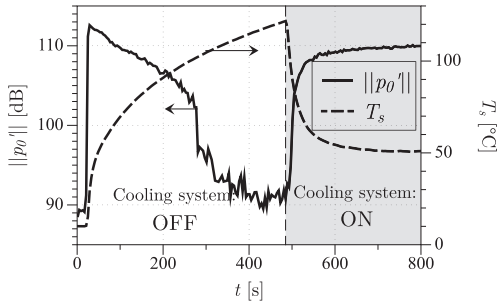

Fig. 3. Experimental evidence of the effect of wall temperature on the amplitude of combustion instabilities: acoustic pressure fluctuation and slot temperature versus time. The flame is ignited at $t = 20$ s, without the cooling system, which is turned on at $t = 480$ s.

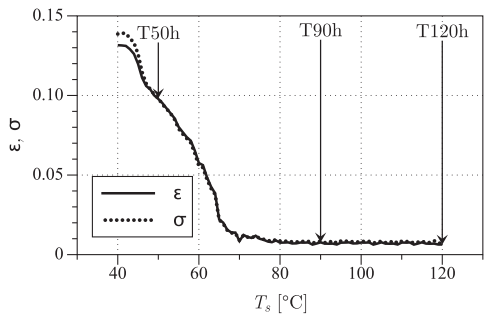

Fig. 4. Influence of slot temperature, T_s on the magnitude of velocity and heat release rate fluctuations, ϵ and σ, respectively. Steady-state test where T_s is controlled via the cooling-water temperature, T_w.

where ω_0 is the Helmholtz mode pulsation and δ the damping coefficient, both under non-reacting conditions. The relative response of the flame to acoustic velocity perturbations is modeled by an interaction index, n, and a time delay, τ. Note that n and τ are not necessarily constants: they measure the amplitude and phase of the flame transfer function $\mathcal{F}$ (*cf.* Eq. (5)). The factor C is derived from combustion-noise theory [14] and depends on the burner geometry and the operating conditions through

$$C = \frac{A_s}{4\pi h_e}\frac{E-1}{r} \tag{2}$$

where A_s is the slot outlet area, $h_e = h_s + e$ the effective height of the slot (e is an end-correction for acoustic waves) and E is the ratio of the fresh to the burnt-gases density. The distance, r, between the noise source and the burner outlet is difficult to evaluate. Here, we define the source as the location where the flame pinches [13]. The numerical values used to compute C are recalled in Table 1.

With the assumption that the pulsation, ω, is close to the Helmholtz mode, ω_0, of the burner, Eq. (1) can be simplified as:

$$[1 + Cn\ \cos(\omega_0\tau)]\omega^2 + i\omega[2\delta + Cn\ \omega_0 \sin(\omega_0\tau)] - \omega_0^2 = 0 \tag{3}$$

which is a second-order polynomial equation. The combustion is unstable if the imaginary part of ω is positive, which according to Eq. (3), is equivalent to

$$n\ \sin(\omega_0\tau) < -\frac{2\delta}{\omega_0 C} \tag{4}$$

Equation 4 is a linear stability criterion, which indicates that in the presence of dissipation (*i.e.* $\delta \neq 0$), the occurrence of a combustion instability depends on both the phase-lag, $\omega_0\tau$, and the magnitude, n, of the flame response.

The resolution of Eq. (1) requires the determination of four parameters:

1. ω_0 and δ, which are related to the acoustic properties of the burner.
2. n and τ, which account for the flame response.

These parameters are evaluated experimentally in Section 5 in order to predict the stability map of the apparatus with respect to the slot temperature, T_s.

Table 1
Numerical values for the evaluation of the combustion-noise parameter C (Eq. (2)).

A_s [m^2]	e [m]	E [−]	r [m]	C [−]
10^{-3}	10^{-2}	7.07	0.022	0.274

5. Experimental results

5.1. Burner acoustics

The determination of $\omega_0 = f_0/2\pi$ and δ is conducted under non-reacting conditions with a bulk velocity of air in the slot $\bar{v} = 1.6$ m/s. Two methods are considered:

1. *Impulse response (IR)*: a short impulse is delivered by the loudspeaker at the bottom of the plenum and the velocity signal is recorded with the hot wire. The response of the system is presented in Fig. 5. An optimal fit with the analytical solution of Eq. (1) (taking $n = 0$) yields the values of f_0 and δ, given in Table 2.
2. *Harmonic response (HR)*: the signal of microphones M_0 and M_1 are simultaneously recorded while a harmonic perturbation is applied via a loudspeaker, outside of the burner. The ratio of the power spectral densities (PSD) is presented in Fig. 6 versus the excitation frequency: the maximum corresponds to the value of f_0 and the half-maximum width to δ/π. The corresponding values are also reported in Table 2.

The two methods give exactly the same value for the Helmholtz frequency but not for the dissipation. This experimental difficulty is known to be one of the weakest points of the prediction of combustion instabilities. For the validation of Section 5.3 an intermediate value between the IR and HR methods is used for the dissipation. A discussion on the sensitivity of the stability map to uncertainties in model parameters is beyond the scope of this paper.

Under non-reacting conditions, the slot temperature is controlled by flowing hot water in the 'cooling' passages (*cf.* Fig. 2). Consequently, values of T_s larger than 100 °C could not be reached. Nevertheless, both acoustic characteristics of the burner proved to be independent of the slot temperature.

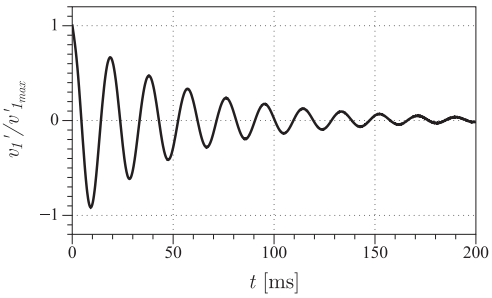

Fig. 5. Impulse response of the system under non-reacting conditions with a bulk velocity $\bar{v} = 1.6$ m/s. Hot-wire probe normalized velocity fluctuation signal $v_1'/v_{1_{max}}'$.

Table 2
Experimental values for the resolution of Eq. (1). Acoustic parameters, ω_0 and δ are determined under non-reacting conditions, either with the impulse-response (IR) or the harmonic response (HR) methodologies.

			T_s [°C]		
			50	90	120
Acoustics	f_0 [Hz]	IR	52		
		2 M	52		
	δ [s_{-1}]	IR	16.9		
		2 M	15.7		
FTF	n		0.87	0.77	0.75
	φ		3.56	3.43	3.33

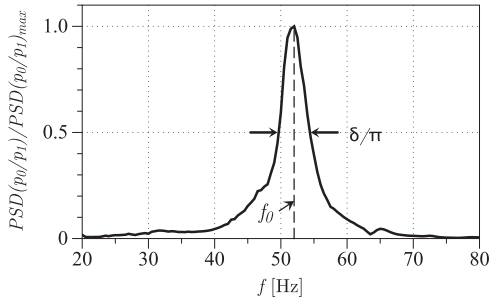

Fig. 6. Two-microphone method for the determination of the acoustic parameters ω_0 and δ under non-reacting conditions. Ratio of the power spectral densities of microphones M_0 and M_1.

5.2. Flame transfer function

The response of the flame to acoustic perturbations is represented by a Flame transfer function (FTF), which is the ratio of the relative heat release rate perturbations, $\dot{q}'/\bar{\dot{q}}$, to the upstream velocity fluctuations, $v'/\bar{v}$. For linear-stability analysis, the FTF is a function of a single variable: the pulsation ω. In order to predict limit-cycle amplitudes and more complex phenomena, the dependance to the amplitude of the velocity fluctuation may be added, resulting in a so-called Flame Describing Function (FDF) [15,11,16,17]. Here, we explore how the FTF may depend on the slot temperature:

$$\mathcal{F}(\omega, T_s) = \frac{\dot{q}'/\bar{\dot{q}}}{v'/\bar{v}} = ne^{i\varphi} \tag{5}$$

where $\varphi = \omega\tau$ is the phase difference associated with the time delay of the flame.

Measuring the complex number $\mathcal{F}(\omega, T_s)$, requires a stable configuration that can be pulsated. For this purpose, it is sufficient to increase the height of the slot to $h_s = 150$ mm. Indeed, the resulting decrease in the Helmholtz frequency brings this configuration back to an unconditionally stable region. The forcing signal is generated by the loudspeaker. The explored frequency range is [10, 300] Hz. Heat release rate and velocity fluctuations are recorded simultaneously by the photomultiplier (PM) and the hot-wire probe (HW) represented in Fig. 1, respectively. The level of rms velocity fluctuation is kept constant at $\varepsilon = 10\%$ of the bulk velocity for all frequencies, which corresponds to the value observed in the self-sustained oscillation test when the slot is cold (*cf.* Fig. 4). The bulk velocity and equivalence ratio are $\bar{v} = 1.6$ m/s and $\Phi = 0.95$, respectively. The cooling system allows to control the wall temperature in the range T_s=48–150 °C. Three relevant temperatures were chosen to measure the FTF: $T_s = 50$, 90 and 120 °C. These operating conditions are labeled T50h, T90h and T120h, respectively.

The amplitude and phase of the FTF are presented in Fig. 7. For all slot temperatures, the gain features a characteristic low-pass-filter shape and the phase grows almost lineally with the frequency. However, as T_s is increased, n decreases for frequencies below 100 Hz while it increases past 100 Hz. The potential causes for this peculiar behavior are discussed in Section 6. The phase, φ, is however marginally affected despite a slight

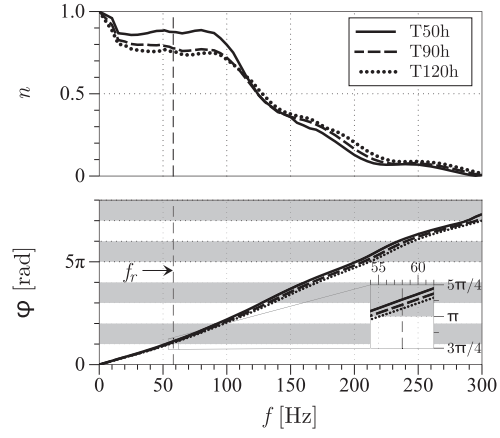

Fig. 7. Flame transfer function. Top: gain, bottom: phase, for three wall temperatures T50h, T90h and T120h. Flow velocity and equivalence ratio are $\bar{v} = 1.6$ m/s and $\Phi = 0.95$ respectively. Velocity fluctuation is keep constant for all frequencies at $\varepsilon = 0.10$.

decrease as T_s increases. This behavior is consistent with previous findings that the phase of the flame response is mostly controlled by the flame height [18,7]. Indeed, thanks to the dual-channel cooling system (*cf.* Fig. 2), the increase in slot temperature has very little impact on the fresh gases resulting in virtually identical flame height. For cases T90h and T120h, the decrease in flame height relative to case T50h are 0.5% and 1.7%, respectively.

The unstable zones corresponding to a case without dissipation (*i.e.* Eq. (4) with $\delta = 0$) are shaded in Fig. 7. At the Helmholtz-mode frequency, the three values of T_s correspond to an unstable condition. However, as reported in Fig. 4, only the case T50h should be unstable. As discussed in Section 5.1, the damping δ and Helmholtz pulsation ω_0 are not affected by the slot temperature. Therefore, Eq. (4) hints that the mechanism responsible for the stabilization is the decrease of n when T_s is increased. The underlying mechanisms of this decrease are discussed in Section 6.

5.3. Validation of the analytical model

The values of n, τ, and f_0 given in Table 2 are used for a numerical resolution of Eq. (1). For the dissipation, we use $\delta = 16$, which is between the IR and HR values.[1] The solution is the complex-valued pulsation, $\omega = \omega_r + i\,\omega_i$, which is reported in Table 3 for the three cases. The low-order model is consistent with the experimental observation (*cf.* Fig. 7) that the flame is unstable for case T50h whereas it is stable for T90h and T120h.

This results shows the ability of low-order models – or more generally acoustic solvers using a FTF to describe the flame response – to account for additional parameters, such as the slot temperature. Despite their versatility, these methods still require input parameters, which can only be obtained through experiments or detailed numerical simulations.

6. Flame-root dynamics

In this section we investigate the mechanisms that may be responsible for the modification of the flame response by the slot temperature. Theoretical and experimental studies have shown how the response of conical flames is essentially controlled by the flame aspect ratio [18–20]. However, in the present configuration, it has been observed that the flame height and shape are marginally affected by changes in T_s, which is due to the limited impact of the slot temperature on the fresh gases temperature (*cf.* Section 5.2).

Table 3
Numerical determination of $\omega = \omega_r + i\,\omega_i$ from Eq. (1) for three values of the slot temperature T_s. The experimental observation of the stability is inferred from Fig. 4.

Case	ω_r [rad/s]	ω_i [rad/s]	Experiment
T50h	369	2.45	Unstable
T90h	366	−6.27	Stable
T120h	365	−11.22	Stable

Nevertheless, multiple studies show that flames nearby a solid surface respond differently to acoustic perturbation, depending on the surface temperature [21–27]. We therefore seek how the flame-root region, which is close to the solid boundary, may alter the flame response. Recent work on conical flames [28] explains how the FTF is the sum of two contributions, one from the flame-root motion and the other one from the interaction of the flame front with a convective perturbation. We propose to explore experimentally how the slot temperature affects the flame-root movement.

6.1. Experimental technique

A flame-front detection algorithm is designed to track the flame root during the harmonic excitation. The flame-root location is chosen as the intersection of the crest of light intensity with the iso-contour at 65% of the maximum pixel value over the whole image. A typical image is presented in Fig. 8.

6.2. Flame root movement

The phase-averaged location of the flame base is presented in Fig. 9, at the frequency f_r of the instability. The coordinates (x', y') are relative to the location of the flame root without excitation, which means that the influence of T_s on the mean flame-root position has been removed from Fig. 9. For the three values of the burner-rim temperature, the horizontal flame displacement is virtually identical and equal to 0.85 mm. However, the vertical displacement is reduced, at least by a factor 3 when T_s increases from 50 to 120 °C. Qualitatively, it means that for this frequency, when the slot is hot, the flame base is more resilient to acoustic velocity perturbations.

Together with the theoretical developments of [28], this behavior of the flame root sheds light on the influence of T_s on the gain of the FTF presented in Fig. 7. The damping of the flame-root movement at f_r, translates into a diminution of the FTF gain.

[1] The stability map is the same with both methods except that with the IR value, case T50h has a lower amplification rate and with the HR value, case T90h is marginally damped.

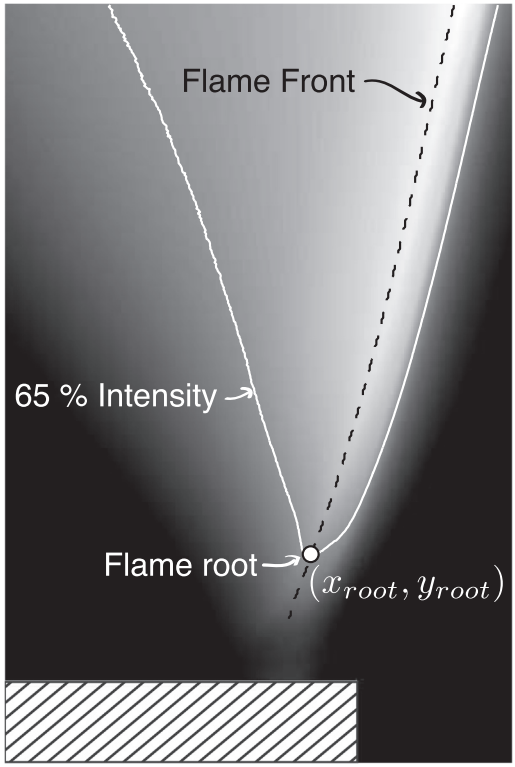

Fig. 8. Typical phase-averaged image for the determination of the flame-root location.

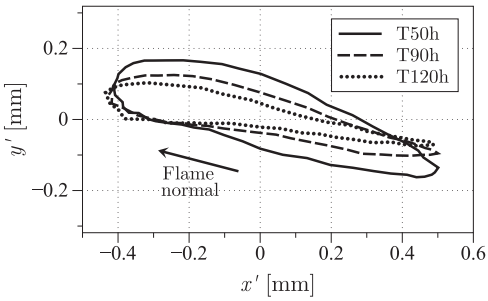

Fig. 9. Phase-averaged flame base trajectory, relative to the flame root position without excitation, at the frequency, f_r, of the instability.

6.3. Flame root transfer function

The trajectories plotted in Fig. 9 are only representative of one frequency. The experiment is replicated over the frequency range [10, 200] Hz and a flame-root transfer function is devised. In the theoretical developments for the flame response, only the displacement normal to the flame front is relevant. Consequently, the gain and phase of the flame-root displacement normal to the mean flame angle (based on the slot width and the flame height) are presented in Fig. 10. For all values of T_s, the gain is small at low and high frequencies and presents a single peak between 100 Hz and 120 Hz. The frequency at the peak increases with T_s. The location of this peak versus the pulsation frequency is related to the flame stand-off distance and it is discussed in [23] for a different setup. The most interesting feature is that while for frequencies below 120 Hz the gain decreases with increasing T_s, the opposite trend is observed past 120 Hz. This feature replicates the trends observed on the FTF in Fig. 7, strongly suggesting that the alteration of the flame-root movement by the burner-rim temperature is the key to the modification of the global flame response.

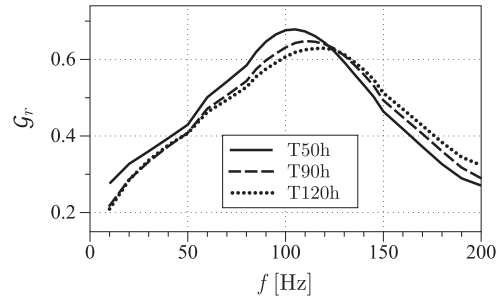

Fig. 10. Gain of the flame-root displacement normal to the mean flame position.

7. Conclusion

A laminar premixed flame stabilized on a slot burner has been investigated experimentally, which exhibits a combustion instability dependent on the temperature of the burner at the flame anchoring point. When the slot is cold, the flame is unstable but as it heats up the instability is damped. Flame transfer functions for various burner-rim temperatures were measured showing that the phase of the FTF is marginally affected while its gain is reduced at low frequency and increased at higher frequencies. Together with measurements of acoustic damping in the apparatus, a low-order model that can predict the influence of the burner-rim temperature on the stability was derived. Finally, the influence of temperature on the FTF was attributed to the dynamics of the flame root at the anchoring point and its dynamic interaction with heat transfer in the material.

Acknowledgment

The authors would like to thank Daniel Durox from Ecole Centrale Paris for his insights on flame dynamics.

References

[1] T. Lieuwen, *Unsteady Combustor Physics*, Cambridge University Press, 2012.
[2] F.E.C. Culick, P. Kuentzmann, *Unsteady Motions in Combustion Chambers for Propulsion Systems*, NATO Research and Technology Organization, 2006.
[3] L. Boyer, J. Quinard, *Combust. Flame* 82 (1) (1990) 51–65.
[4] T. Schuller, D. Durox, S. Candel, *Combust. Flame* 128 (2002) 88–110.
[5] H. Wang, C. Law, T. Lieuwen, *Combust. Flame* 156 (4) (2009) 889–895.
[6] A. Cuquel, D. Durox, T. Schuller, *7th Mediterranean Combustion Symposium* (2011) 1–2.
[7] R.S. Blumenthal, P. Subramanian, R. Sujith, W. Polifke, *Combust. Flame* 160 (7) (2013) 1215–1224.
[8] L. Selle, T. Poinsot, B. Ferret, *Combust. Flame* 158 (1) (2011) 146–154.
[9] R. Price, I. Hurle, T. Sudgen, *Proc. Combust. Inst.* 12 (1968) 1093–1102.
[10] D. Durox, T. Schuller, S. Candel, *Proc. Combust. Inst.* 29 (2002) 69–75.
[11] N. Noiray, D. Durox, T. Schuller, S. Candel, *J. Fluid Mech.* 615 (2008) 139–167.
[12] D. Durox, T. Schuller, N. Noiray, A. Birbaud, S. Candel, *Combust. Flame* 155 (3) (2008) 416–429.
[13] T. Schuller, D. Durox, S. Candel, *Combust. Flame* 135 (2003) 525–537.
[14] P. Clavin, E.D. Siggia, *Combust. Sci. Technol.* 78 (1991) 147–155.
[15] T. Lieuwen, S. Preetham, *AIAA Paper* (4035) (2004) 1–16.
[16] F. Boudy, D. Durox, T. Schuller, S. Candel, *Proc. Combust. Inst.* 33 (2011) 1121–1128.
[17] P. Palies, D. Durox, T. Schuller, S. Candel, *Combust. Flame* 158 (10) (2011) 1980–1991.
[18] T. Schuller, D. Durox, S. Candel, *Combust. Flame* 134 (2003) 21–34.
[19] V. Kornilov, K. Schreel, L. de Goey, *Proc. Combust. Inst.* 31 (2007) 1239–1246.
[20] V. Kornilov, R. Rook, P.D. Goey, *Proc. Combust. Inst.* 1 (3) (2009) 1–6.
[21] M. Fleifil, A. Annaswamy, Z. Ghoneim, A. Ghoniem, *Combust. Flame* 106 (4) (1996) 487–510.
[22] K. Schreel, R. Rook, L. de Goey, *Proc. Combust. Inst.* 29 (2002) 115–122.
[23] R. Rook, L.D. Goey, L. Somers, K. Schreel, R. Parchen, *Combust. Theory Model.* (2002) 37–41.
[24] R. Rook, L. de Goey, *Combust. Flame* 133 (1-2) (2003) 119–132.
[25] H. Altay, S. Park, D. Wu, D. Wee, A. Annaswamy, A. Ghoniem, *Proc. Combust. Inst.* 32 (1) (2009) 1359–1366.
[26] K. Kedia, H. Altay, A. Ghoniem, *Proc. Combust. Inst.* 33 (2011) 1113–1120.
[27] L. de Goey, J. van Oijen, V. Kornilov, J. ten Thije Boonkkamp, *Proc. Combust. Inst.* 33 (2011) 863–886.
[28] A. Cuquel, D. Durox, T. Schuller, *Comptes Rendus Mécanique* 341 (2013) 171–180.